Supplemental Materials

Loss of hepatic DRP1 exacerbates alcoholic hepatitis by inducing megamitochondria and mitochondrial maladaptation

Xiaowen Ma[1], Allen Chen[1], Luma Melo[2], Ana Clemente-Sanchez[2,3], Xiaojuan Chao[1], Ali Reza Ahmadi[4], Brandon Peiffer[4], Zhaoli Sun[4], Hiromi Sesaki[5], Tiangang Li[6], Xiaokun Wang[7,8], Wanqing Liu[7,8], Ramon Bataller[2], Hong-Min Ni[1] and Wen-Xing Ding[1*]

1. Department of Pharmacology, Toxicology and Therapeutics, University of Kansas Medical Center, Kansas City, KS 66160, USA

2. Center for Liver Diseases, Division of Gastroenterology, Hepatology and Nutrition, University of Pittsburgh Medical Center, Pittsburgh, PA, USA

3. Liver Unit and Digestive Department, Hospital General Universitario Gregorio Marañon. CIBERehd, Instituto de Salud Carlos III. Madrid, Spain.

4. Department of Surgery, Johns Hopkins School of Medicine, Baltimore, MD 21205, USA

5. Department of Cell Biology, Johns Hopkins University School of Medicine, Baltimore, MD 21205, USA

6. Harold Hamm Diabetes Center, Department of Physiology, University of Oklahoma Health Sciences Center, Oklahoma City, OK 73104, USA

7. Department of Pharmaceutical Sciences, Eugene Applebaum College of Pharmacy and Health Sciences; Wayne State University, Detroit, MI 48201, USA

8.Department of Pharmacology, School of Medicine, Wayne State University, Detroit, MI 48201, USA

Supplemental Materials and Methods

Chronic plus binge (Gao-binge) alcohol feeding

This was done as described previously with minor modifications. Briefly, mice were acclimated to the Lieber-DeCarli liquid control diet (F1259SP; Bio-Serv, Flemington, NJ) for 5 days followed by further feeding with the liquid control or ethanol diet (5% ethanol; F1258SP; Bio-Serv) for 10 days. The volume of the control diet given to mice was matched to the volume of ethanol diet consumed. In Cox8-GFP-mCherry assay, 1 dose of adenovirus-Cox8-GFP-mCherry ($2x10^8$ PFU/mouse, intravenously [IV]) was given on the day before ethanol feeding. On the last day of feeding, mice also were given ethanol 5 g/kg or maltose dextran 9 g/kg and sacrificed 8 hours later.

RNA extraction and RNA amplification

Total RNA was extracted from human or mouse livers using TRIzol reagent (15596-026; Ambion, ThermoFisher Scientific) and was reverse-transcribed into cDNA using RevertAid Reverse Transcriptase (EP0442; Fermentas, ThermoFisher Scientific).

For RNA sequencing analysis, total RNA samples were quality checked with a Qubit assay for RNA quantification and Agilent TapeStation gel analysis for RNA quality. Sequencing libraries were constructed using 1 µg of total RNA using the NEBNext Ultra II Directional RNA Library Prep Kit for Illumina (NEB). The sequencing library construction process includes mRNA purification by the polyA tails with polyT magnetic beads, fragmentation, strand-specific cDNA synthesis, end repair, 3’ end adenylation, adapter ligation, and PCR amplification. The constructed sequencing libraries were validated and quantified with Qubit and TapeStation assays. The sequencing library preps were pooled together equally by ng amount and the nM concentration of the pool was verified with an Illumina KAPA Library Quantification qPCR assay

(Roche). Each library was indexed with a barcode sequence and sequenced in a multiplexed fashion. An Illumina NextSeq 550 system was used to generate single-end, 75-base sequence reads from the libraries. Base calling was carried out by the instrument's Real-Time Analysis (RTA) software. The base call files (bcl files) were demultiplexed and converted to compressed FASTQ files by bcl2fastq2.

Quantitative PCR was performed using SYBR Green chemistry (1725124; Bio-Rad). Primer sequences (5'–3') used in the present study were listed in **Supplemental Table 2**. All the results were normalized to 18s and expressed as fold change over the Control group.

RNAseq data analysis

The RNAseq data were analyzed using our previously established technical pipeline [1, 2]. Briefly, we used HISAT2 v.2.1.0.13 to map the high-quality reads to the mouse reference genome (GRCm38.90). Quantification of the gene expression was generated with HTSeq-counts v0.6.0. Significant differentially expressed genes (DEGs) were generated with the R package DESeq2. Statistical significance was calculated by adjusting the P values with the Benjamini-Hochberg's false discovery rate (FDR) [3].

The clustered heatmaps of the cGAS-STING pathway genes were plotted with ClustVis [4] (PMID). Principle component analysis (PCA) and volcano plots were prepared with R. Pathway analysis were performed by using Ingenuity Pathway Analysis (IPA). We analyzed the enrichment of up-and down-regulated genes among each knock-out (KO) group as compared to the wild-type (WT) group and each EtOH as compared to the control group. Genes with a log2 fold change >1.5 or <-1.5 with an FDR-corrected q value <0.05 were used to perform the analysis.

Liver metabolomics analysis

Metabolomics analysis was performed by Metabolon. The present dataset comprises a total of 907 compounds of known identity (named biochemicals). Following log transformation and imputation of missing values, if any, with the minimum observed value for each compound, Welch's two-sample t-test was used to identify biochemicals that differed significantly between experimental groups. A summary of the numbers of biochemicals that achieved statistical significance ($p \leq 0.05$), as well as those approaching significance ($0.05 < p < 0.10$) is shown.

Measurement of Liver Triglyceride

To determine the abundance of lipid droplets in liver specimens, we stained frozen hepatic tissue with Oil Red O as previously described [5]. In addition, hepatic triglyceride (TG) extraction was performed as described previously [6]. Briefly, approximately 20–50 mg of liver tissue was ground into powder in liquid nitrogen using a mortar and pestle. TGs were extracted by incubating the powdered tissue in 1 mL chloroform-methanol (2:1) mixture for 1 hour at room temperature with vigorous shaking. ddH_2O 200 μL was added to the samples followed by a brief vortex and 3,000g centrifugation for 5 min to separate the lipid phase. The lower lipid phase was collected and dried overnight, and the remaining pellet was dissolved in a tert-butanol, Triton X-114, and methanol (9:4:2) mixture. TG levels were measured by colorimetric assay using a kit from Pointe Scientific (Canton, MI; T7532-500) according to the manufacturer's instructions.

Cellular Fractionation and Western Blot analysis

Total liver lysates were prepared using radioimmunoprecipitation assay (RIPA) buffer (1% NP40, 0.5% sodium deoxycholate, 0.1% sodium dodecyl (lauryl) sulfate). Nuclear and cytoplasmic fractions were purified using a commercial kit (Thermo scientific, 78835) Heavy membrane (HM, contains mitochondria) and cytosol fraction were prepared from fresh liver tissue as described previously [7]. Briefly, liver tissues were homogenized in HIM buffer (200 mM

mannitol,70 mM sucrose, 5 mM Hepes, 0.5 mM EGTA (pH 7.5) containing 1% protease inhibitors) using a dounce homogenizer. Homogenates were centrifuged at 1000×g to remove debris, and the supernatant was centrifuged at 10,000×g for 10 min to separate HM and cytosolic fractions. The supernatant was kept as the cytosolic fraction, and the pellet was further washed by centrifugation and re-suspended in HIM buffer as the HM fraction. To determine the levels of mitochondrial oxidative phosphorylation (OXPHOS) proteins, 30 μg of protein were mixed with the loading buffer at room temperature without heat boiling. All the other proteins were determined with heat boiling. Proteins (30μg) were separated by 8%–12% SDS-PAGE gel before transfer to a PVDF membrane. Membranes were probed using indicated primary and secondary antibodies and developed with SuperSignal West Pico Plus Chemiluminescent Substrate (Thermo scientific, 34579) and Immobilon Western Chemiluminescent HRP Substrate (Millipore, WBKLS0500). All the primary and secondary antibodies used in this study were listed in **Supplemental Table 3**.

Electron Microscopy

Fine-cut liver tissues were fixed with 2% glutaraldehyde in phosphate buffer 0.1 mol/L (pH 7.4) followed by 1% OsO_4. After dehydration, thin sections were stained with uranyl acetate and lead citrate for observation under a JEM 1016CX electron microscope (JEOL, Tokyo, Japan). Images were acquired digitally.

Cox8-GFP-mCherry assay for mitophagy in vitro and in vivo

To detect mitophagy in vivo, cryo-sectioned liver tissue from mice with Cox8-GFP-mCherry overexpression was further stained with Hoechst 33342 (1μg/ml) and imaged with Nikon A1R confocal microscope. Images were acquired digitally using an oil lens at 100x. More than 5 images were taken from one mouse liver section and the number of red-only puncta in each cell was counted in more than 18 cells per mouse from 3 different mice. For in vitro assay, murine

hepatocytes were isolated according to the methods described previously.[8] Cells were cultured in Williams Medium E and maintained in a 37 °C incubator with 5% CO_2. To examine mitophagy, primary hepatocytes were seeded in a 12 well-plate (2 x 10^5 in each well) and infected with adenovirus-Cox8-GFP-mCherry (10 MOI) for 24 h. Cells were fixed with 4% paraformaldehyde in phosphate-buffered saline (PBS) and kept at 4 °C for microscopy. Fluorescence images were acquired using Nikon A1R confocal microscope.

Measurement of Mitochondria Bioenergetic Function

This assay was performed as we recently reported [9]. Briefly, mouse livers were homogenized in mitochondria isolation buffer (70 mM sucrose, 210 mM mannitol, 5 mM HEPES, 1 mM EGTA, and 0.5% (w/v) fatty acid-free BSA; pH 7.2). Homogenates were centrifuged twice at 1000×g for 10 min at 4 °C and the supernatants were centrifuged once at 8000×g for 10 min at 4 °C. The mitochondrial pellets were suspended in the isolation buffer and total proteins were determined using BCA protein assay. All mitochondrial respiration assays were performed using an XF24x3 Extracellular Flux Analyzer by Seahorse Bioscience (North Billerica, Massachusetts). Mitochondria from 2 to 4 mice/group were pooled and the assays were done in triplicate. Isolated liver mitochondria were suspended in cold mitochondrial assay solution (1×MAS: 70 mM sucrose, 220 mM mannitol, 10 mM KH_2PO_4, 5 mM $MgCl_2$, 2 mM HEPES, 1 mM EGTA and 0.2% (w/v) fatty acid-free BSA, pH 7.2 at 37 °C) containing substrate (10 mM succinate + 2 µM rotenone) to a final concentration of 0.2 mg/ml protein, and 50 µl mitochondrial suspension was plated to each well (except for background correction wells). The plate was centrifuged at 2000×g for 20 min at 4 °C and 450 µl of 1× MAS-substrate solution was added to each well. The sensor cartridge was loaded with port A, 40 mM ADP (4 mM final); port B, 25 µg/ml oligomycin (2.5 µg/ml final); port C, 40 µM FCCP (4 µM final); and port D, 40 µM antimycin A (4 µM final) to measure the bio-energetic profile. The plate was pre-warmed to 37 °C and transferred to the

XF24 instrument after calibration. The respiration was measured in a coupled state with substrate present (basal respiration), followed by State 3 (phosphorylating respiration, in the presence of ADP and substrate), State 4o (leak state induced with the addition of oligomycin - an inhibitor of ATP synthase), and then maximal uncoupler (FCCP)-stimulated respiration (State 3u). At the end, antimycin A (complex III inhibitor) is added to inhibit mitochondrial respiration completely.

Hepatocytes, non-parenchymal cells, and Kupffer cells isolation

Mouse hepatocytes and non-parenchymal cells were isolated by retrograde, non-recirculating perfusion of liver with 0.05% Collagenase Type IV (Sigma, C5138) as described previously [10]. Red blood cells were removed from non-parenchymal cells fraction using Red Blood Cell lysing Buffer (Sigma, R7757) as manufacturer's instruction. Kupffer cells were further separated from non-parenchymal cells using gradient Percoll (GE Healthcare, 17-0891-01) centrifugation as described previously [11].

Immunohistochemical Staining

Neutrophil accumulation in the liver was assessed by myeloperoxidase (MPO) staining with a standard immunohistochemistry procedure. Briefly, paraffin-embedded tissue sections were incubated with primary antibody at 4°C overnight after deparaffinization and heat-induced antigen retrieval in citrate buffer. Sections were then washed and incubated with secondary antibody for 1h at 37°C and developed by use of ImmPACT NovaRED HRP substrate (Vector Labs, SK-4805). Tissues were counterstained with hematoxylin. The number of MPO-positive cells was counted from 15 different fields (100X) in a double-blinded fashion. Similar procedures were used for the immunohistochemical staining of IRF7, and STING. For Sirius Red staining, paraffin-embedded liver tissue sections were dewaxed and rehydrated followed by staining sections with Sirius Red Solution. The positive areas of Sirius Red staining were quantified For

Sirius Red Staining

Paraffin-embedded liver tissue sections were dewaxed and rehydrated followed by staining sections with Sirius Red Solution. The positive areas of Sirius Red staining were quantified using Image J (NIH) software.

Immunofluorescence Staining

Cryo-sectioned liver tissue was permeabilized in 0.2% Triton X-100/PBS for 15 min, followed by blocking in 2% BSA/PBS for 1 h. Cells were incubated with primary antibodies overnight in a humidified chamber at 4°C followed by extensive washing before the addition of secondary antibodies for 1 h at room temperature. Slides were mounted in PermaFluor Aqueous Mounting Medium (Thermo Scientific, TA-030-FM) followed by confocal microscopy. For double-color immunofluorescence, two first antibodies (CD68 and GS) were co-incubated followed by Alexa Fluor 488/549 secondary antibodies.

Detection of mtDNA release

Mouse hepatocytes were isolated from WT and L-DRP1 KO mice fed with Gao-binge alcohol respectively. Cytosolic extracts were purified using the digitonin method as previously described [12]. Briefly, $1x10^6$ hepatocytes suspension was divided into two equal aliquots, and one aliquot was resuspended in 500 µl of 50 µM NaOH and boiled for 30 minutes to solubilize DNA. 50µl 1M Tris-HCl pH 8 was added to neutralize the pH, and these extracts served as normalization controls for total mtDNA. The second equal aliquots were resuspended in 500 µl buffer containing 150 mM NaCl, 50 mM HEPES, pH 7.4, and 25 µg/ml digitonin (Millipore, 300410). The homogenates were incubated end over end for 10 minutes to allow selective plasma membrane permeabilization, then centrifuged at 980 g for 3 min three times to pellet intact cells. The cytosolic supernatants were transferred to fresh tubes and spun at 17000 g for 10 min to

pellet any remaining cellular debris, yielding cytosolic fraction free of nuclear, mitochondrial, and ER contamination. DNA was then isolated from these pure cytosolic fractions and whole cell extracts using QIAQuick Nucleotide Removal Columns (QIAGEN, 28306). Quantitative real-time PCR was performed on both whole-cell extracts and cytosolic fractions using mtDNA primers (Dloop1-3, ND1, 16S), and levels of mtDNA from whole-cell extracts served as normalization controls. To detect mtDNA in blood, total DNA was isolated from the equal volume of mouse serum using DNeasy Blood & Tissue Kits (QIAGEN, 69504) followed by Quantitative real-time PCR with mtDNA primers.

Luciferase Reporter Assay

Luciferase reporter plasmids containing around 2000bp mouse Dnm1l promoter sequence (-2003/+143, relative to transcription start site) were generated using T4 DNA ligase (Thermo Scientifics, EL0011) following the manufacture's instruction. $2x10^5$ primary mouse hepatocytes were infected with Ad-TFEB or Ad-null in 0.5-1 MOI and seeded in a 24-well plate for 24 hours. 1ug reporter plasmids were transfected for another 24 hours using Lipofectamine 2000 (Thermo Scientific, 10660027). Luciferase intensity was detected at the 48h from seeding with Promega Luciferase Assay Kit (Promega, E1500) following the manufacturer's protocol. Results were shown as fold change to the control group.

Chromatin Immunoprecipitation Assay

Pooled chow-fed WT mouse livers (n=3) were used for ChIP assay. Assay was performed with anti-TFEB antibody (Bethyl Laboratoryies, A303-673A, 10 µg/ ml final concentration), Normal rabbit IgG (Cell Signaling Technology, 2729S, 10 µg ml−1 final concentration) as a negative control, Dynabeads™ Protein G magnetic beads (Thermo-Fisher Scientific, 10003D), and a ChIP assay kit (Millipore,17-295) following the manufacturer's instruction [13]. The sequence of ChIP real-time PCR primers were listed in **Supplemental Table 2.**

TUNEL Staining

Terminal deoxynucleotidyl transferase dUTP nick end labeling (TUNEL) staining was performed in paraffin-embedded liver sections using the In Situ Cell Death Detection TUNEL Kit from Roche (ROCHE-11684809910) follow the manufacturer's instruction.

Liver Cytokines/ Chemokines Detection

Pooled liver lysate from Gao-binge alcohol-feeding WT and L-DRP1 KO mouse were subjected to mouse cytokine antibody array kit (Cat. ARY006) for the detection of 40 different cytokines and chemokines (n=4 mice).

Statistical Analysis

All experimental data were expressed as mean ± SE and subjected to one-way ANOVA analysis with Bonferroni post hoc test or Student t-test where appropriate. Mean ± SD were used for the quantitative data. A p-value less than 0.05 was considered significant.

Supplemental Table 1 Characteristics of the AH patients

ID	Age	Sex	BMI	ETOH Duration (years)	Diagnosis	MELD	ALT (U/L)	AST (U/L)	Creatinine (mg/dL)	Albumin (g/dL)	Bilirubin (mg/dL)	AP (U/L)	PT	INR	WBC (K/cu mm)	Hemoglobin (g/dL)	Platelets (K/cu mm)	Sepsis
AH51	50	F	28.60	38	Acute Alcoholic Hepatitis	38	14	55	2.4	4.2	39.9	61	24	2.5	13.37	7.7	102	No
AH52	48	F	34.92	29	Acute Alcoholic Hepatitis	36	86	158	4.3	3.8	28	227	15.4	1.5	28.91	10.3	158	Yes
AH53	47	M	28.69	31	Alcoholic Cirrhosis	32	36	97	1.5	2.6	28.5	182	22.3	2.3	29.59	7.2	31	No
AH54	39	F	26.51	23	Acute Alcoholic Hepatitis	32	30	62	1.8	4.2	24.9	184	22.7	2.3	17.06	6.9	95	No
AH55	60	M	31.40	43	Alcoholic Cirrhosis	26	44	115	1.6	2.3	9.1	123	18.8	1.9	14.66	7	41	Yes
AH58	58	M	29.30	30	Alcoholic Cirrhosis	17	32	70	1.14	2.6	4.4	112	14.3	1.4	6.51	10.9	84	No
AH63	62	M	32.32	24	Acute Alcoholic Hepatitis	44	81	84	4.5	2.8	36.2	73	24.7	2.4	30.93	9.5	20	Yes
AH72	33	M	30.26	6	Acute Alcoholic Hepatitis	36	29	110	2.4	2.3	23	99	24.1	2.3	33.74	10.6	323	No
AH77	32	M	31.81	1	Acute Alcoholic Hepatitis	50	108	162	6.9	4.2	46.9	285	25.6	2.5	22.51	15	141	No

BMI, body mass index; MELD, model for end-stage liver disease; ALT, alanine aminotransferase; AST, aspartate aminotransferase; AP, alkaline phosphatase; PT, prothrombin time; INR, international normalized ratio; WBC, white blood cell

Supplemental Table 2 List of Primers Used for Real-Time PCR

Gene	Forward primer (5'-3')	Reverse primer (5'-3')
18s	GAGCGAAAGCATTTGCCAAG	GGCATCGTTTATGGTCGGAA
hDNM1L	CAAAGCAGTTTGCCTGTGGA	TCTTGGAGGACTATGGCAGC
hMFN1	CCTGGCATCCAGGAGTTAGA	TGGTTCCAGCAATGCGATTT
hMFN2	TGCAGGTGTAAGGGACGATT	GAGGCTCTGCAAATGGGATG
hCGAS	CACGTATGTACCCAGAACCC	GTCCTGAGGCACTGAAGAAAG
hIRF7	CAGATCCAGTCCCAACC	GTCTCTACTGCCCACCCGTA
hIFNA1	GACTCCATCTTGGCTGTGA	TGATTTCTGCTCTGACAACCT
hIFNB1	ATGACCAACAAGTGTCTCCTCC	GCTCATGGAAAGAGCTGTAGTG
hIRF3	TCTGCCCTCAACCGCAAAGAAG	TACTGCCTCCACCATTGGTGTC
mDnm1l	GGAGAAGAAAATGGAGTTGAAGCA	TGACAACGTTGGGCGAGAA
mMfn1	ACTCAGTAAACGTGGCAGCA	TCCTCCGTGACCTCCTTGAT
mMfn2	AGGGCTCGGAGAAGGTATGT	CTCAGTGGCAAGAAGGGAGG
mActa2	GTCCCAGACATCAGGGAGTAA	TCGGATACTTCAGCGTCAGGA
mCol1a1	TGTGTTCCCTACTCAGCCGTCT	CATCGGTCATGCTCTCTCCAA
mTgfb1	TGCTAATGGTGGACCGCAA	CACTGCTTCCCGAATGTCTGA
mCgas	GTCGGAGTTCAAAGGTGTGGA	GACTCAGCGGATTTCCTCGTG
mIrf7	CAATTCAGGGGATCCAGTTG	AGCATTGCTGAGGCTCACTT
mIfit1	CAAGGCAGGTTTCTGAGGAG	GACCTGGTCACCATCAGCAT
mIfit3	TTCCCAGCAGCACAGAAAC	AAATTCCAGGTGAAATGGCA
mIfi44	CTGATTACAAAAGAAGACATGACAGAC	AGGCAAAACCAAAGACTCCA
mIsg15	CTAGAGCTAGAGCCTGCAG	AGTTAGTCACGGACACCAG
mCxcl10	CCAAGTGCTGCCGTCATTTTC	GCTCGCAGGGATGATTTCAA
mIfnb1	CCCTATGGAGATGACGGAGA	CCCAGTGCTGGAGAAATTGT
mIfna4	CTTTCCTCATGATCCTGGTAATGAT	AATCCAAAATCCTTCCTGTCCTTC
mCd68	TGCGGCTCCCTGTGTGT	TCTTCCTCTGTTCCTTGGGCTAT
mIl1b	GCCCATCCTCTGTGACTCAT	AGGCCACAGGTATTTTGTCG
mTnf	CGTCAGCCGATTTGCTATCT	CGGACTCCGCAAAGTCTAAG
mCcl2	ACATTCGGCGGTTGCTCTAG	ACATCCTGTATCCACACGGCAG
mCcl4	AACACCATGAAGCTCTGCGT	AGAAACAGCAGGAAGTGGGA
mCxcl2	CTCAGAGGAAGACGATGAAG	GACGAGTTATCCCAGCCAAA
mIcam1	CAATTTCTCATGCCGCACAG	AGCTGGAAGATCGAAAGTCCG
mVcam1	TGAACCCAAACAGAGGCAGAGT	GGTATCCCATCACTTGAGCAGG
mTfeb	CCAGAAGCGAGAGCTCACAGAT	TGTGATTGTCTTTCTTCTGCCG
msXbp1	GGTCTGCTGAGTCCGCAGCAGG	AGGCTTGGTGTATACATGG
muXbp1	ACGGCCTTGTGGTTGAGAAC	TGTCCATTCCCAAGCGTGTT
mHspa5	AGTGGTGGCCACTAATGGAG	CAATCCTTGCTTGATGCTGA
mDdit3	CAGGAGGTCCTGTCCTCAGA	CTCCTGCTCCTTCTCCTTCA
mDnajb9	CCCCAGTGTCAAACTGTACCAG	AGCGTTTCCAATTTTCCATAAATT
ChIP (distal)	CTGGATCTTCAGAGTCTTTC	GGTTACTTACCATTCACCTG
ChIP (proximal)	TTTGCGCGCCCACCTCTGT	AGCAGGCCACTGCAATGAATG
mtLoop1	AATCTACCATCCTCCGTGAAACC	TCAGTTTAGCTACCCCCAAGTTTAA

mtLoop2	CCCTTCCCCATTTGGTCT	TGGTTTCACGGAGGATGG
mtLoop3	TCCTCCGTGAAACCAACAA	AGCGAGAAGAGGGGCATT
mt16s	CCGCAAGGGAAAGATGAAAGAC	TCGTTTGGTTTCGGGGTTTC
mtNd1	CAGGATGAGCCTCAAACTCC	GGTCAGGCTGGCAGAAGTAA

Supplemental Table 3 List of antibodies used for western blot, IHC and immunofluorescence staining

Antibodies	**Brand**	**Catalogue Number**
AIF	Abcam	ab32516
ASS1	Proteintech	16210-1-AP
β-actin	Sigma	A5441
BIP	Sigma	G9043
cd68	Biolegend	137002
cGAS	Cell Signaling	31659
CHOP	Santa Cruz	Sc-793
cytochrome C	Pharmigen	556433
DRP1	BD Bioscience	611112
eIF2	Cell Signaling	9722
p-eIF2	Cell Signaling	9721s
TFEB	Bethyl	A303-673A
GAPDH	Cell Signaling	2118
Glutamine Synthase	Abcam	ab176562
HNF4α	R&D	P-H1415-00
IRF3	Cell Signaling	4302
p-IRF3 (Ser396)	Cell Signaling	29047
IRF7	Cell Signaling	72073
Lamin A/C	Cell Signaling	2032

LC3	N/A	N/A
Mfn1	Santa Cruz	sc-50330
Mfn2	Sigma	M6444
Myeloperoxidase (MPO)	BioCare medical	PP023AA
Oxphos Cocktail	abcam	110413
p62	Abnova	H00008878-M01
Parkin	Santa Cruz	sc32282
PGC1α	Abnova	PAB12061
STING	Cell Signaling	50494S
TBK1	Cell Signaling	3504
p-TBK1(Ser172)	Cell Signaling	5483
Tom20	Santa Cruz	sc-11415
TIM23	BD Bioscience	611222
Ubiquitin	Santa Cruz	sc-8017
HRP-Goat Anti-Mouse IgG	Jackson	115-035-146
HRP-Goat Anti-Rabbit IgG	Jackson	111-035-144
Rhodamine Red Goat Anti-Rat	Jackson	112-295-167
Alex594 Goat Anti-mouse	Jackson	115-585-003
Alex488 Goat Anti-Rabbit	Jackson	111-545-144
HRP Horse Anti-Rabbit IgG	Vector	MP7401

Supplemental Figures

Supplemental Figure 1

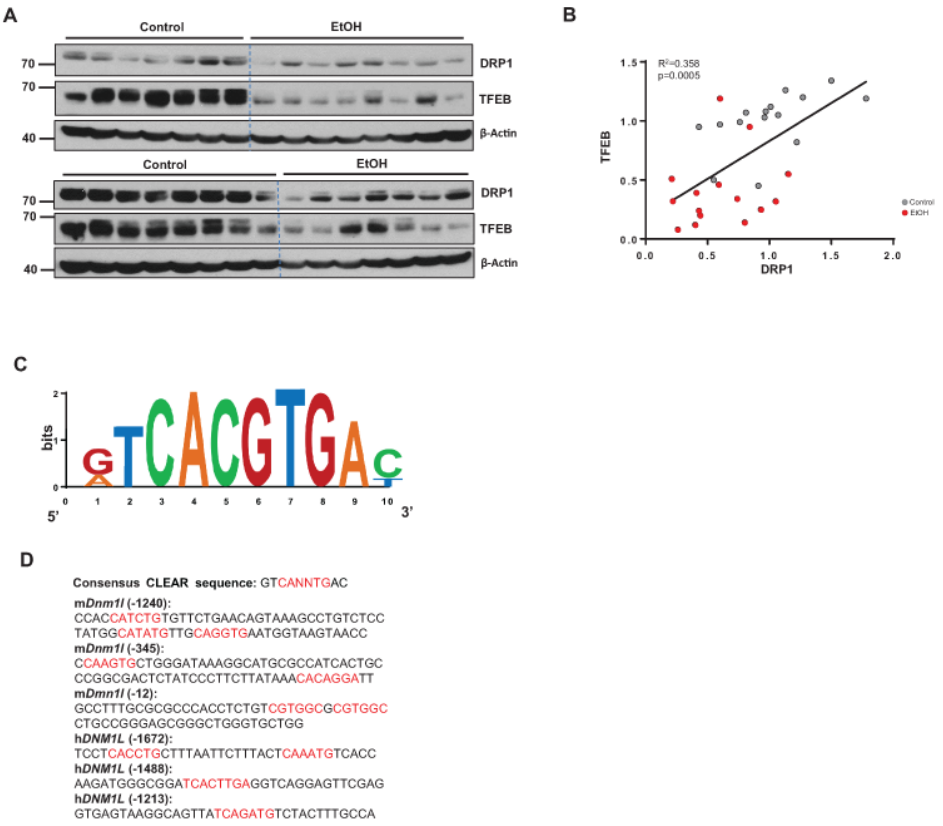

Figure S1. TFEB binds to DNM1L gene promoter. (A) Immunoblot analysis for DRP1 and TFEB with total liver lysates from Gao-binge alcohol-fed mice. (B) Correlation analysis of DRP1 and TFEB expression in (A). (C) Logo representation of the consensus CLEAR sequence for TFEB binding sites. (D) Anticipated CLEAR sequence location relative to the transcriptional start site of mouse and human DNM1L (DRP1) gene were indicated in red.

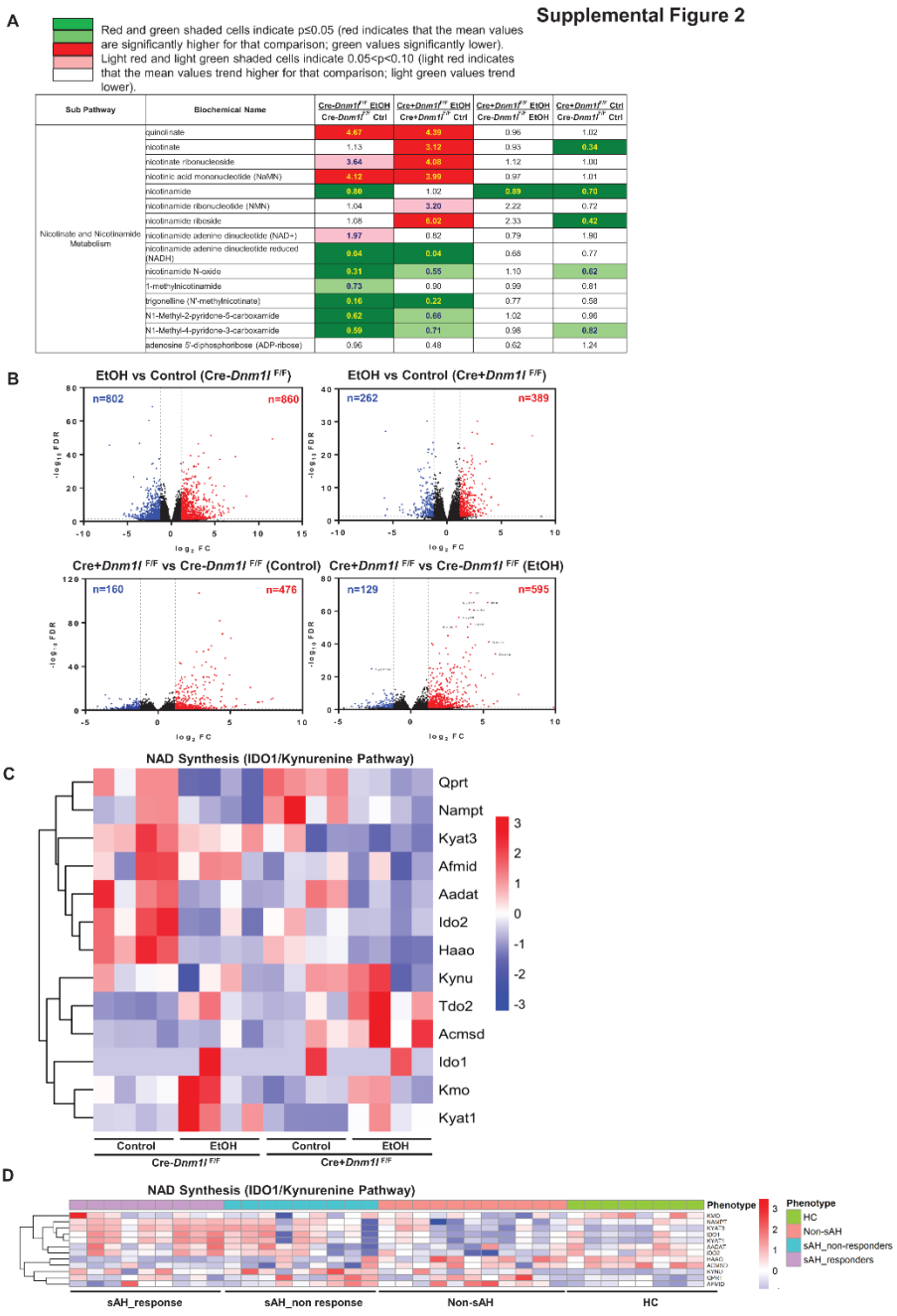

Figure S2. Liver NAD metabolism and synthesis pathway in Gao-Binge alcohol-fed mice and AH human patients. (A) Heatmap of Nicotinate and Nicotinamide metabolites in metabolomics analysis of indicated mouse liver tissues (n=6). (B) Volcano plot of RNA-seq analysis. Heapmap analysis of NAD synthesis pathway involved genes from RNA-seq dataset of indicated mouse liver tissues (C, n=4) and human healthy and AH patient livers (D, n=8-11) . HC, healthy control; Non-sAH, non-severe alcoholic hepatitis; sAH_non response, severe alcoholic hepatitis but does not respond to steroid treatment; sAH_response, severe alcoholic hepatitis respond to steroid treatment.

Red and green shaded cells indicate p≤0.05 (red indicates that the mean values are significantly higher for that comparison; green values significantly lower). Light red and light green shaded cells indicate 0.05<p<0.10 (light red indicates that the mean values trend higher for that comparison; light green values trend lower).

Supplemental Figure 3

A

Sub Pathway	Biochemical Name	Cre-*Dnm1l*$^{F/F}$ EtOH / Cre-*Dnm1l*$^{F/F}$ Ctrl	Cre+*Dnm1l*$^{F/F}$ EtOH / Cre+*Dnm1l*$^{F/F}$ Ctrl	Cre+*Dnm1l*$^{F/F}$ EtOH / Cre-*Dnm1l*$^{F/F}$ EtOH	Cre+*Dnm1l*$^{F/F}$ Ctrl / Cre-*Dnm1l*$^{F/F}$ Ctrl
Glycolysis, Gluconeogenesis, and Pyruvate Metabolism	1,5-anhydroglucitol (1,5-AG)	0.88	0.73	0.99	1.19
	glucose	0.36	0.47	0.83	0.63
	glucose 6-phosphate	0.20	0.14	0.69	0.97
	fructose 1,6-diphosphate/glucose 1,6-diphosphate/myo-inositol diphosphates	0.51	0.37	0.83	1.15
	2,3-diphosphoglycerate	1.68	1.39	1.00	1.21
	dihydroxyacetone phosphate (DHAP)	0.18	0.43	1.09	0.46
	2-phosphoglycerate	1.53	1.08	1.25	1.77
	3-phosphoglycerate	1.06	0.79	1.35	1.81
	phosphoenolpyruvate (PEP)	1.25	0.90	1.49	2.05
	pyruvate	0.70	0.71	1.27	1.26
	lactate	0.43	0.54	1.12	0.90
	glycerate	1.33	1.81	0.94	0.69

B

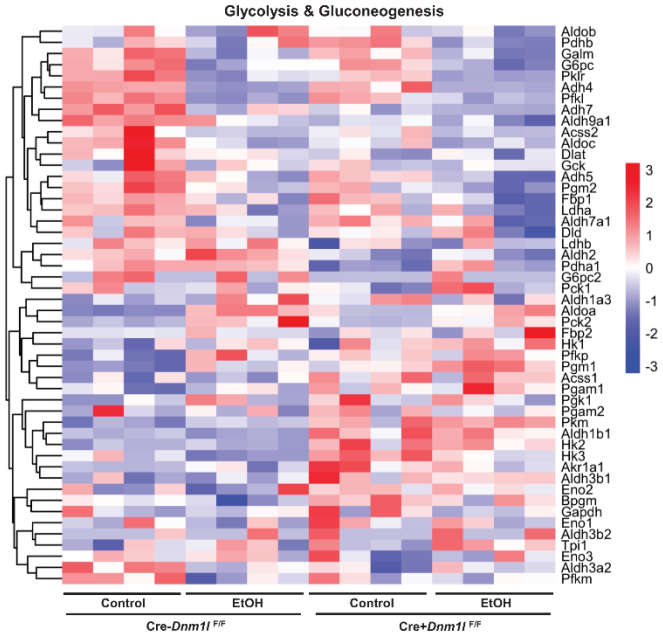

C

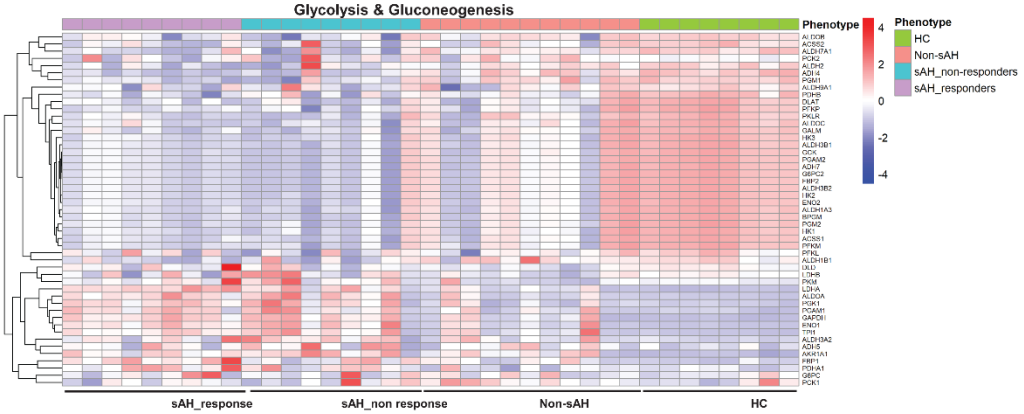

Figure S3. Liver glucose metabolism pathway in Gao-Binge alcohol-fed mice and AH human patients. (A) Heatmap of glucose metabolism of metabolomics analysis of indicated mouse liver tissues (n=6). Heapmap analysis of glycolysis and gluconeogenesis pathway involved genes from RNA-seq dataset of indicated mouse liver tissues (B, n-4), and human healthy and AH patient livers (C, n=8-11) . HC, healthy control; Non-sAH, non-severe alcoholic hepatitis; sAH_non response, severe alcoholic hepatitis but does not respond to steroid treatment; sAH_response, severe alcoholic hepatitis respond to steroid treatment.

Supplemental Figure 4

A

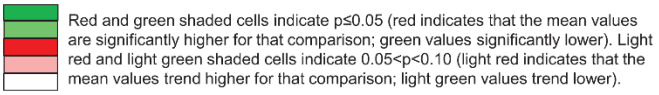

Sub Pathway	Biochemical Name	Cre-*Dnm1l*$^{F/F}$ EtOH / Cre-*Dnm1l*$^{F/F}$ Ctrl	Cre+*Dnm1l*$^{F/F}$ EtOH / Cre+*Dnm1l*$^{F/F}$ Ctrl	Cre+*Dnm1l*$^{F/F}$ EtOH / Cre-*Dnm1l*$^{F/F}$ EtOH	Cre+*Dnm1l*$^{F/F}$ Ctrl / Cre-*Dnm1l*$^{F/F}$ Ctrl
TCA Cycle	citrate	2.46	1.03	0.74	1.78
	aconitate [cis or trans]	2.61	1.30	0.69	1.38
	alpha-ketoglutarate	0.91	1.24	1.10	0.81
	succinylcarnitine (C4-DC)	0.47	0.28	1.05	1.78
	succinate	0.99	0.86	1.19	1.36
	fumarate	0.79	1.16	1.43	0.98
	malate	0.74	1.09	1.35	0.91
	itaconate	1.37	1.35	3.51	3.56
	tricarballylate	0.16	0.47	1.01	0.34
	2-methylcitrate/homocitrate	1.39	2.03	0.96	0.65
Oxidative Phosphorylation	acetylphosphate	0.58	0.65	1.05	0.93
	phosphate	1.13	1.31	1.05	0.91

B

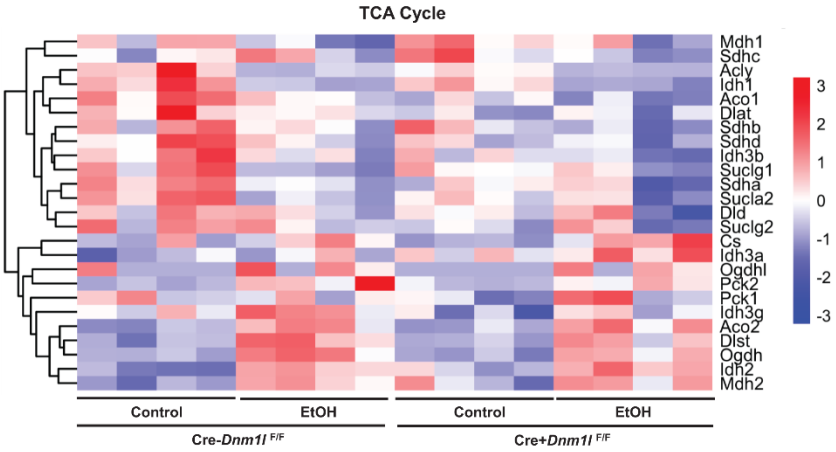

C

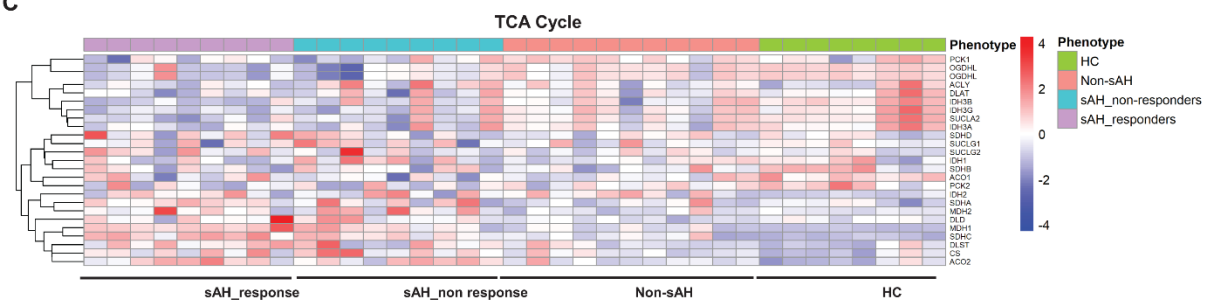

Figure S4. Liver TCA cycle pathway in Gao-Binge alcohol-fed mice and AH human patients. (A) Heatmap of TCA cycle and oxidative phosphorylation metabolites of metabolomics analysis of indicated mouse liver tissues (n=6). Heapmap analysis of TCA cycle involved genes from RNA-seq dataset of indicated mouse liver tissues (B, n-4), and human healthy and AH patient livers (C, n=8-11) . HC, healthy control; Non-sAH, non-severe alcoholic hepatitis; sAH_non response, severe alcoholic hepatitis but does not respond to steroid treatment; sAH_response, severe alcoholic hepatitis respond to steroid treatment.

Supplemental Figure 5

A

Red and green shaded cells indicate p≤0.05 (red indicates that the mean values are significantly higher for that comparison; green values significantly lower). Light red and light green shaded cells indicate 0.05<p<0.10 (light red indicates that the mean values trend higher for that comparison; light green values trend lower).

Sub Pathway	Biochemical Name	Cre-*Dnm1l*$^{F/F}$ EtOH / Cre-*Dnm1l*$^{F/F}$ Ctrl	Cre+*Dnm1l*$^{F/F}$ EtOH / Cre+*Dnm1l*$^{F/F}$ Ctrl	Cre+*Dnm1l*$^{F/F}$ EtOH / Cre-*Dnm1l*$^{F/F}$ EtOH	Cre+*Dnm1l*$^{F/F}$ Ctrl / Cre-*Dnm1l*$^{F/F}$ Ctrl
Pentose Metabolism	ribose	0.60	1.29	0.80	0.37
	ribitol	0.35	1.12	1.08	0.34
	ribonate	0.25	0.90	1.82	0.50
	ribulose/xylulose	0.47	0.99	0.84	0.40
	arabitol/xylitol	0.78	1.03	1.03	0.78
	arabonate/xylonate	0.74	1.07	0.84	0.58
	sedoheptulose	0.31	0.67	0.78	0.36
	lyxonate	0.69	1.64	0.81	0.34
Glycogen Metabolism	maltohexaose	0.21	0.25	0.78	0.68
	maltopentaose	0.16	0.08	0.32	0.64
	maltotetraose	0.17	0.07	0.25	0.62
	maltotriose	0.23	0.15	0.35	0.54
	maltose	0.36	0.46	0.58	0.44

B

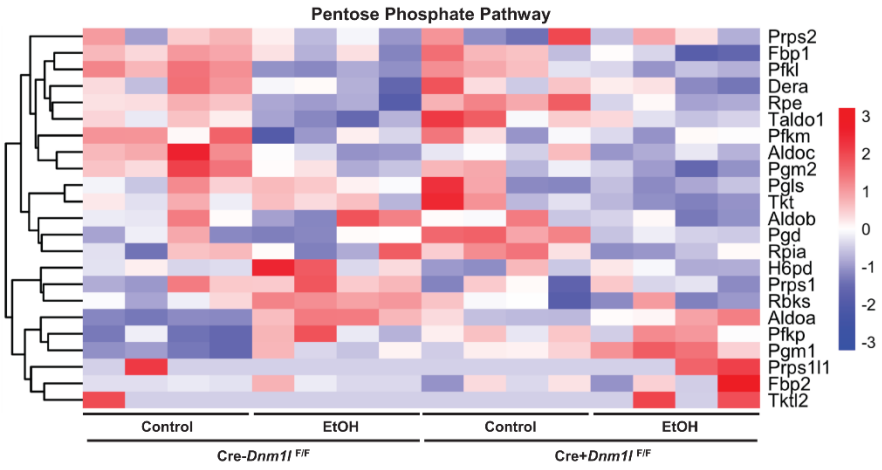

C

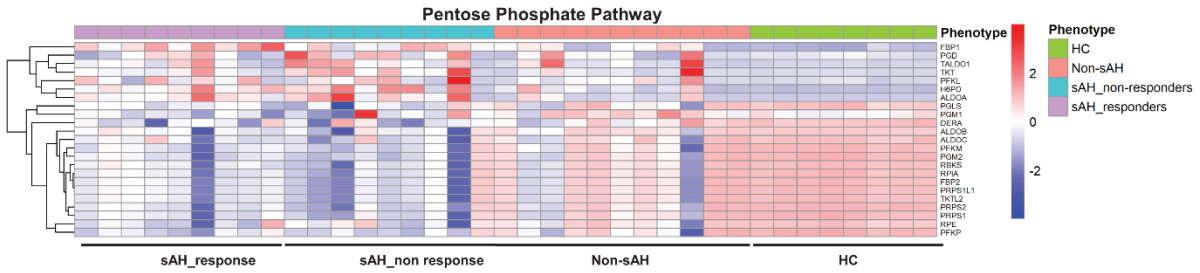

Figure S5. Liver pentose and glycogen metabolism pathway in Gao-Binge alcohol-fed mice and AH human patients. (A) Heatmap of pentose and glycogen metabolites of metabolomics analysis of indicated mouse liver tissues (n=6). Heapmap analysis of pentose phosphate pathway involved genes from RNA-seq dataset of indicated mouse liver tissues (B, n-4), and human healthy and AH patient livers (C, n=8-11) . HC, healthy control; Non-sAH, non-severe alcoholic hepatitis; sAH_non response, severe alcoholic hepatitis but does not respond to steroid treatment; sAH_response, severe alcoholic hepatitis respond to steroid treatment.

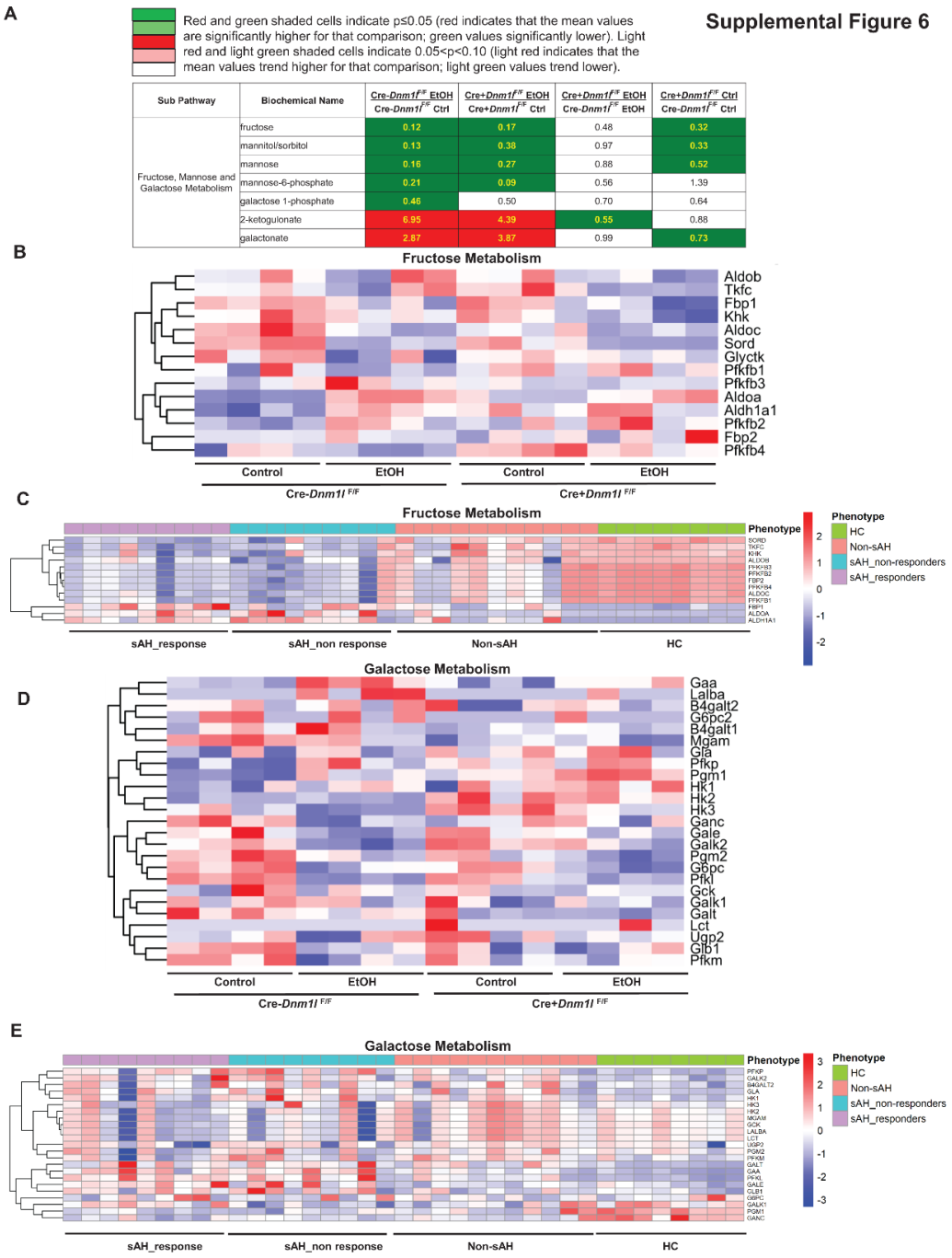

Figure S6. Liver fructose and galactose metabolism pathway in Gao-Binge alcohol-fed mice and AH human patients. (A) Heatmap of fructose and galactose metabolites of metabolomics analysis of indicated mouse liver tissues (n=6). Heapmap analysis of fructose and galactose metabolism pathway involved genes from RNA-seq dataset of indicated mouse liver tissues ((B&D, n-4), and human healthy and AH patient livers (C&E, n=8-11) . HC, healthy control; Non-sAH, non-severe alcoholic hepatitis; sAH_non response, severe alcoholic hepatitis but does not respond to steroid treatment; sAH_response, severe alcoholic hepatitis respond to steroid treatment.

Supplemental Figure 7

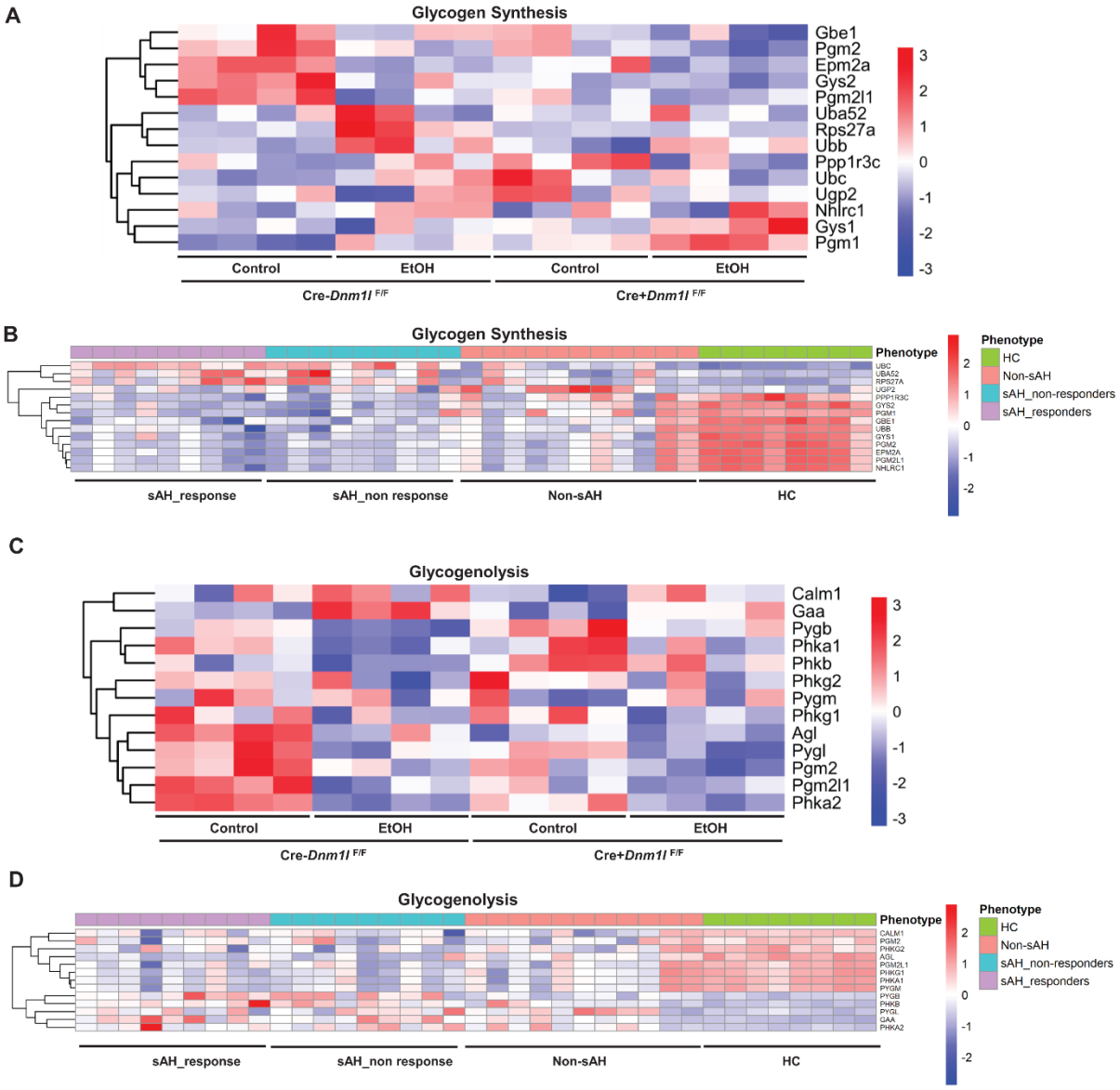

Figure S7. Liver glycogen metabolism pathway in Gao-Binge alcohol-fed mice and AH human patients. Heapmap analysis of glycogen synthesis and glycogenolysis pathway involved genes from RNA-seq dataset of indicated mouse liver tissues (A&C, n-4), and human healthy and AH patient livers (B&D, n=8-11) . HC, healthy control; Non-sAH, non-severe alcoholic hepatitis; sAH_non response, severe alcoholic hepatitis but does not respond to steroid treatment; sAH_response, severe alcoholic hepatitis respond to steroid treatment.

Supplemental Figure 8

A

Red and green shaded cells indicate p≤0.05 (red indicates that the mean values are significantly higher for that comparison; green values significantly lower). Light red and light green shaded cells indicate 0.05<p<0.10 (light red indicates that the mean values trend higher for that comparison; light green values trend lower).

Sub Pathway	Biochemical Name	Cre-*Dnm1l*$^{F/F}$ EtOH / Cre-*Dnm1l*$^{F/F}$ Ctrl	Cre+*Dnm1l*$^{F/F}$ EtOH / Cre+*Dnm1l*$^{F/F}$ Ctrl	Cre+*Dnm1l*$^{F/F}$ EtOH / Cre-*Dnm1l*$^{F/F}$ EtOH	Cre+*Dnm1l*$^{F/F}$ Ctrl / Cre-*Dnm1l*$^{F/F}$ Ctrl
Glutathione Metabolism	glutathione, reduced (GSH)	0.31	0.23	1.12	1.53
	glutathione, oxidized (GSSG)	0.71	0.82	1.40	1.21
	cysteine-glutathione disulfide	0.50	0.96	1.01	0.53
	S-methylglutathione	0.39	0.37	1.28	1.34
	S-lactoylglutathione	0.69	1.73	1.37	0.55
	cysteinylglycine	0.36	0.24	1.12	1.67
	5-oxoproline	1.75	2.20	1.21	0.97
	2-hydroxybutyrate/2-hydroxyisobutyrate	5.35	3.41	0.85	1.33
	ophthalmate	10.59	12.60	1.04	0.87
	S-(1,2-dicarboxyethyl)glutathione	0.85	0.60	2.03	2.88
	4-hydroxy-nonenal-glutathione	0.82	0.87	0.92	0.86
	3'-dephospho-CoA-glutathione*	1.26	1.54	0.76	0.62
	CoA-glutathione^	3.35	1.37	0.52	1.28

B

Sub Pathway	Biochemical Name	Cre-*Dnm1l*$^{F/F}$ EtOH / Cre-*Dnm1l*$^{F/F}$ Ctrl	Cre+*Dnm1l*$^{F/F}$ EtOH / Cre+*Dnm1l*$^{F/F}$ Ctrl	Cre+*Dnm1l*$^{F/F}$ EtOH / Cre-*Dnm1l*$^{F/F}$ EtOH	Cre+*Dnm1l*$^{F/F}$ Ctrl / Cre-*Dnm1l*$^{F/F}$ Ctrl
Methionine, Cysteine, SAM and Taurine Metabolism	methionine	0.83	1.25	1.02	0.68
	N-acetylmethionine	0.90	1.73	1.40	0.73
	N-formylmethionine	1.15	1.25	0.90	0.83
	S-methylmethionine	0.74	0.51	0.73	1.05
	methionine sulfone	0.75	0.44	0.77	1.32
	methionine sulfoxide	1.03	1.91	0.95	0.51
	N-acetylmethionine sulfoxide	1.27	2.17	1.25	0.74
	S-adenosylmethionine (SAM)	0.52	0.36	1.02	1.49
	S-adenosylhomocysteine (SAH)	1.21	1.23	0.94	0.92
	2,3-dihydroxy-5-methylthio-4-pentenoate (DMTPA)*	0.72	0.99	1.85	1.34
	homocysteine	1.43	1.02	1.05	1.48
	cystathionine	0.97	0.53	1.05	1.91
	alpha-ketobutyrate	2.50	2.33	0.96	1.03
	cysteine	0.64	0.53	1.02	1.23
	N-acetylcysteine	0.82	0.89	1.02	0.94
	S-methylcysteine	1.83	2.14	0.75	0.64
	cysteine sulfinic acid	2.17	1.19	1.27	2.32
	hypotaurine	1.28	1.02	1.10	1.38
	taurine	1.31	0.95	1.02	1.42
	N-acetyltaurine	3.53	3.03	1.19	1.39
	succinoyltaurine	0.37	0.70	1.27	0.66
	taurocyamine	1.16	0.95	0.87	1.06
	3-sulfo-L-alanine	2.07	1.65	0.80	1.00

Figure S8. Liver glutathione and methionine metabolism pathway in WT and L-DRP1 KO mice fed with Gao-Binge alcohol. (A) Heatmap of glutathione metabolism of metabolomics analysis of indicated mouse liver tissues. (B) Heatmap of methionine metabolism of metabolomics analysis of indicated mouse liver tissues (n=6).

Supplemental Figure 9

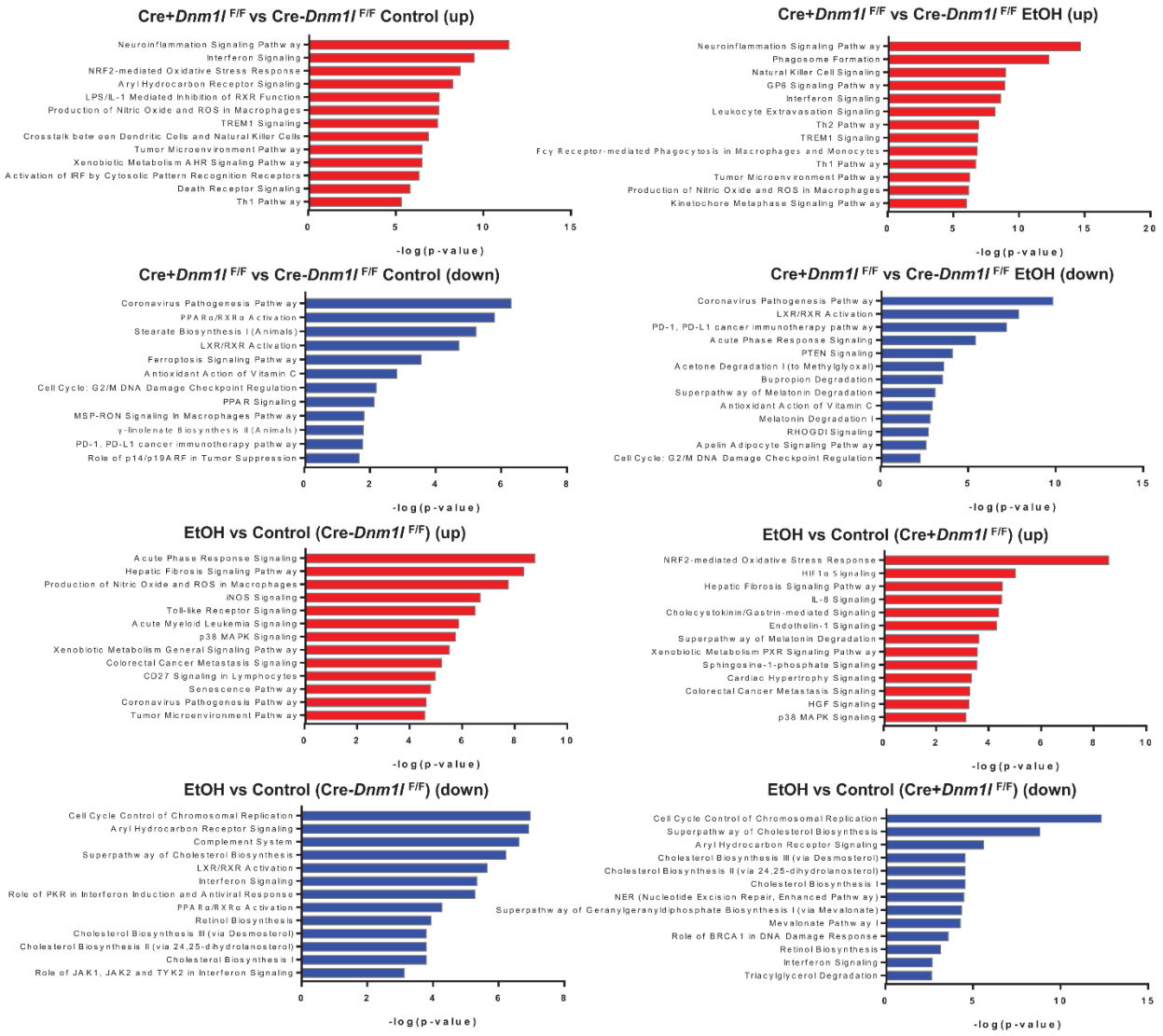

Figure S9. Ingenuity Pathway Analysis of RNA-seq dataset. The top up-and down-regulated pathways identified by Ingenuity Pathway Analysis (IPA) from RNA-seq dataset of indicated mouse liver tissues.

Supplemental Figure 10

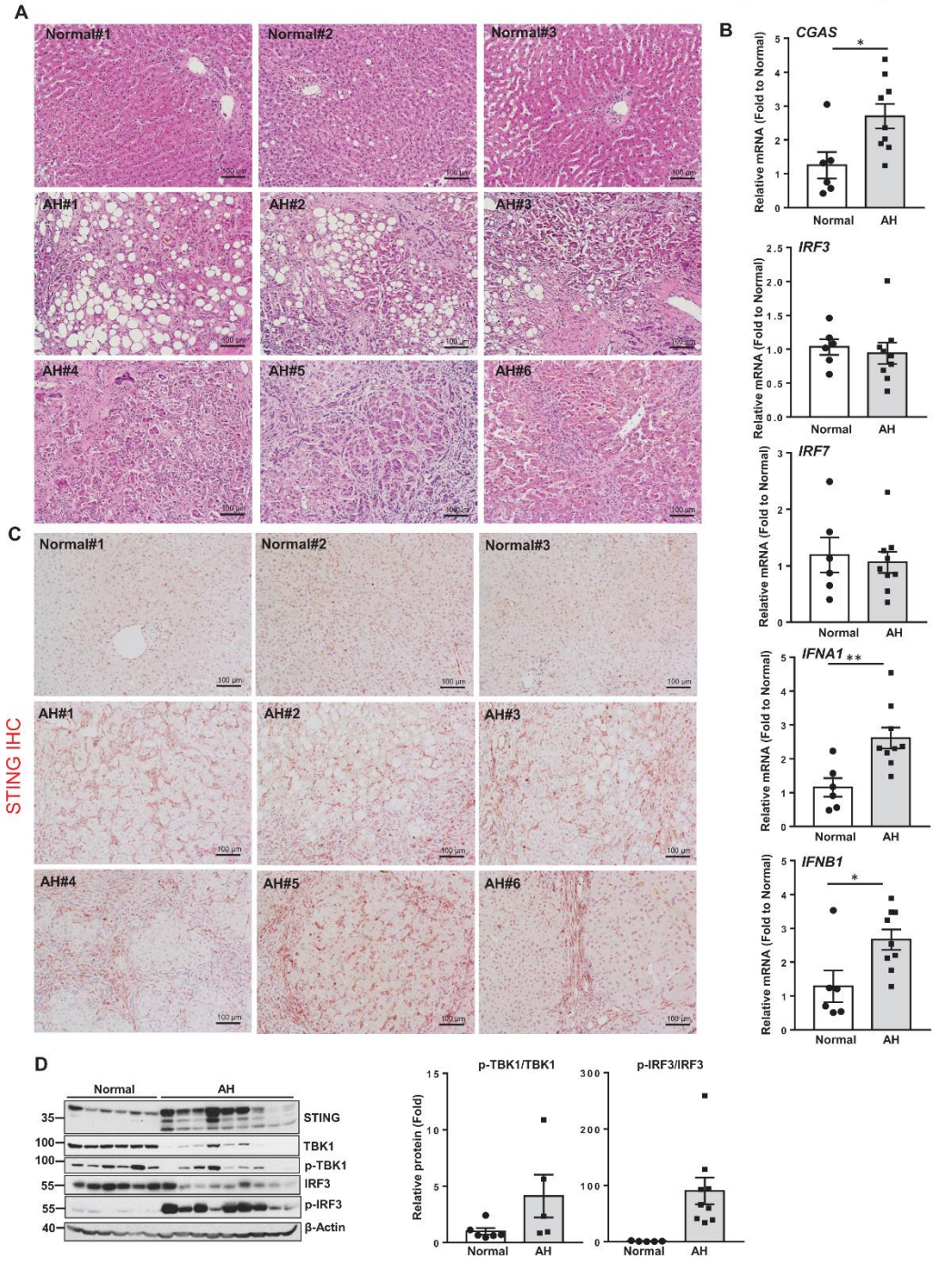

Figure S10. Activated cGAS-IRF pathway in AH human liver. (A) Representative H&E staining of the liver tissue from healthy human donors and patients with AH. (B) Total liver RNA were extracted followed by quantitative real-time PCR analysis (C) IHC staining for STING in paraffin-embedded human liver. (D) Total liver lysates from AH patients and healthy donors were subjected to western blot analysis. All data are presented as means± SEM (n=6-9). *p<0.05, **p<0.01; two-tailed Student's t-test.

Supplemental Figure 11

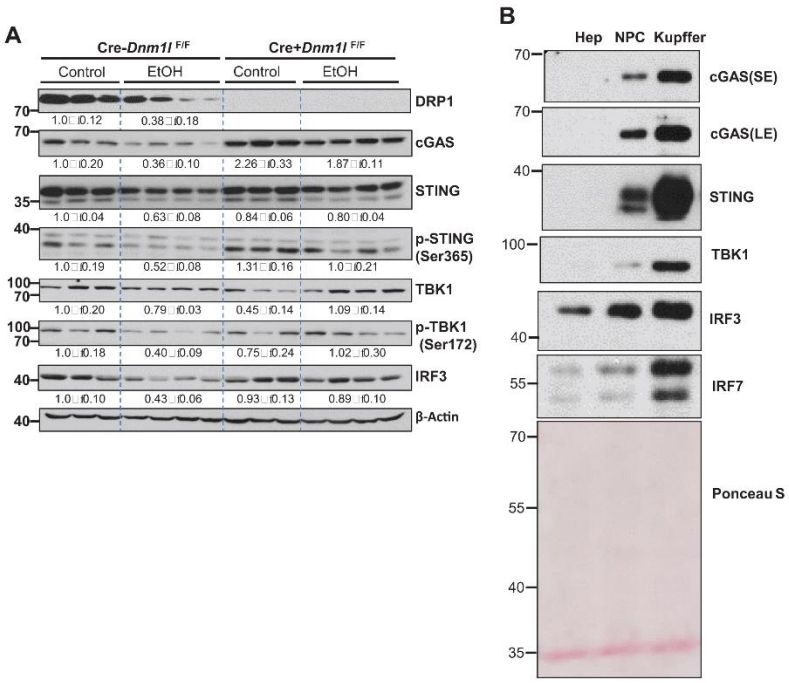

Figure S11. Activated cGAS-IRF pathway in L-DRP1 KO mouse liver. (A) Male WT C57BL/6J mice (2-3-month-old) were subjected to Gao-binge alcohol feeding. Total liver lysates were subjected to western blot analysis.(n=3-4) (B) Indicated types of cell were pufified and total lysed from mouse liver and subjected to western blot analysis.

Supplemental Figure 12

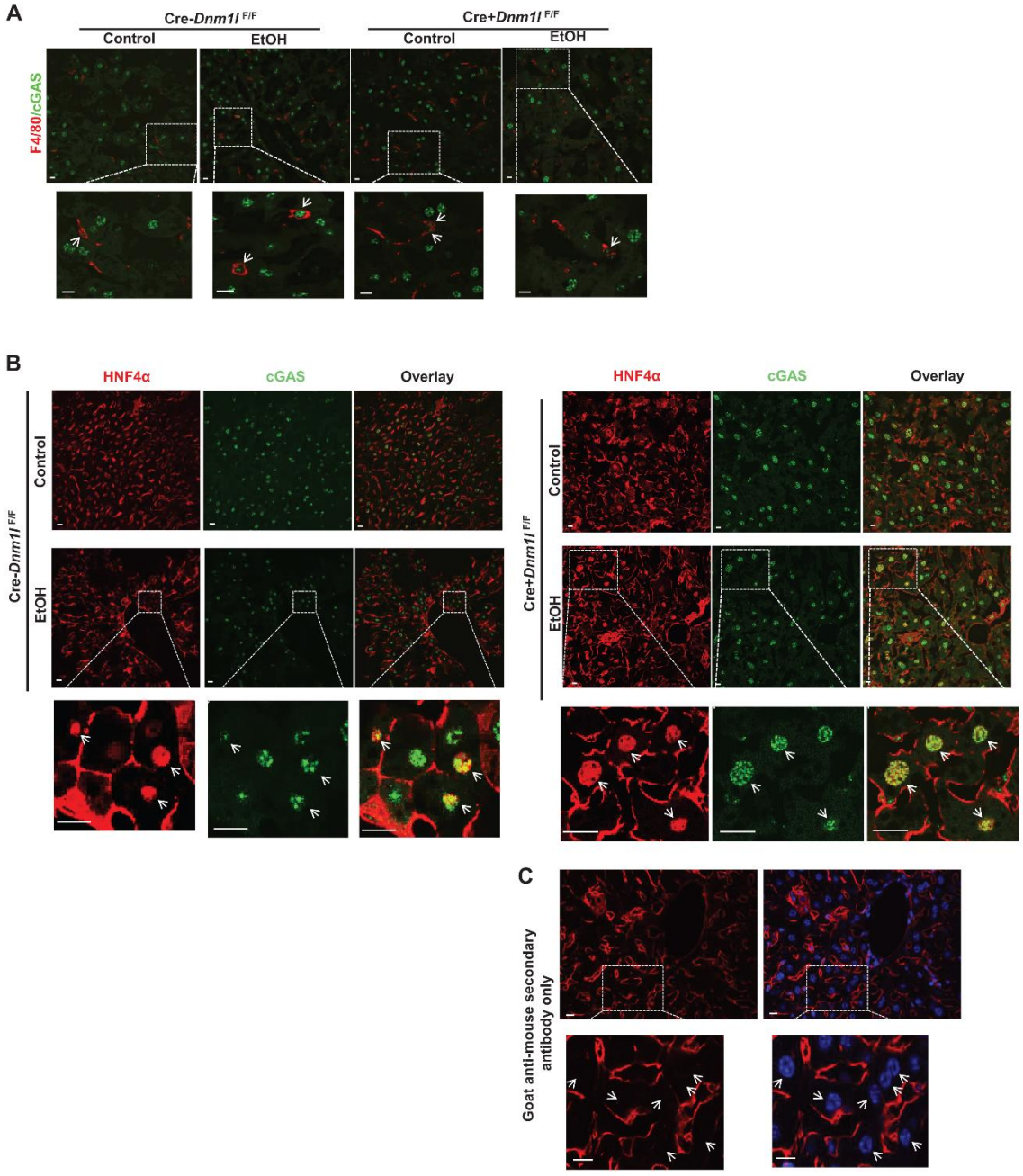

Figure S12. cGAS expression in both hepatocytes and Kuffer cells/ macrophages in mouse liver. (A) Representative images of immunofluorescence staining of F4/80 (red) and cGAS (green) of indicated mouse liver. Arrows denote cGAS positive Kuffer cells /macrophages. (B) Representative images of immunofluorescence staining of HNF4α (red) and cGAS (green) of indicated mouse liver. Arrows denote cGAS positive hepatocytes. (C) Non-specific goat anti-mouse secondary antibody staining showing no nucleus staining.

Supplemental Figure 13

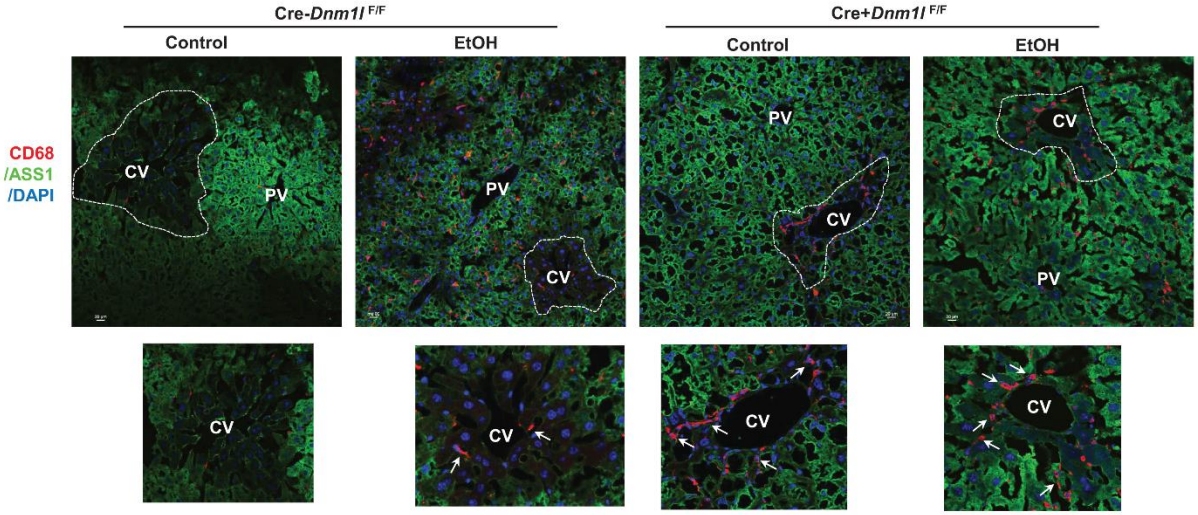

Figure S13. Change of macrophage zonation in the liver of L-DRP1 KO mouse.
Representative images of immunofluorescence staining of CD68 (red) and argininosuccinate synthase 1 (ASS1, green) in indicated mouse liver. Arrows denote macrophages clustered in the central vein region.

Supplemental Figure 14

Red and green shaded cells indicate p≤0.05 (red indicates that the mean values are significantly higher for that comparison; green values significantly lower). Light red and light green shaded cells indicate 0.05<p<0.10 (light red indicates that the mean values trend higher for that comparison; light green values trend lower).

Sub Pathway	Biochemical Name	Cre-*Dnm1l*$^{F/F}$ EtOH / Cre-*Dnm1l*$^{F/F}$ Ctrl	Cre+*Dnm1l*$^{F/F}$ EtOH / Cre+*Dnm1l*$^{F/F}$ Ctrl	Cre+*Dnm1l*$^{F/F}$ EtOH / Cre-*Dnm1l*$^{F/F}$ EtOH	Cre+*Dnm1l*$^{F/F}$ Ctrl / Cre-*Dnm1l*$^{F/F}$ Ctrl
Eicosanoid	prostaglandin F2alpha	0.61	1.16	1.53	0.80
	6-keto prostaglandin F1alpha	0.48	1.49	1.58	0.51
	12-HEPE	3.57	5.67	0.72	0.45
	5-HETE	1.86	4.84	1.27	0.49
	12-HETE	1.47	2.23	1.08	0.72
	15-HETE	1.74	3.05	1.25	0.71
	12-HHTrE	0.84	1.90	1.42	0.63
Endocannabinoid	oleoyl ethanolamide	0.74	1.32	1.05	0.59
	palmitoyl ethanolamide	0.17	0.31	1.14	0.62
	stearoyl ethanolamide	0.23	0.31	0.96	0.71
	N-myristoyltaurine*	4.08	3.99	0.77	0.78
	N-arachidonoyltaurine	0.79	1.59	1.55	0.77
	N-oleoyltaurine	3.09	5.01	1.05	0.65
	N-stearoyltaurine	2.80	3.23	1.03	0.89
	N-palmitoyltaurine	2.11	3.44	1.10	0.67
	N-palmitoleoyltaurine*	1.71	2.81	1.06	0.65
	N-linoleoyltaurine*	3.56	3.74	0.84	0.80
	N-linolenoyltaurine*	5.85	4.65	0.86	1.08
	hexanoyltaurine	3.67	3.91	0.95	0.89
	linoleoyl ethanolamide	3.03	3.94	0.84	0.65
	N-oleoylserine	3.52	3.41	0.54	0.56
	N-stearoylserine*	3.34	2.34	0.58	0.82
	N-palmitoylserine	5.19	2.84	0.55	1.01

Figure S14. Liver eicosanoid and endocannabinoid metabolites in WT and L-DRP1 KO mice fed with Gao-Binge alcohol. Heatmap of eicosanoid and endocannabinoid metabolism of metabolomics analysis of indicated mouse liver tissues (n=6).

Supplemental Figure 15

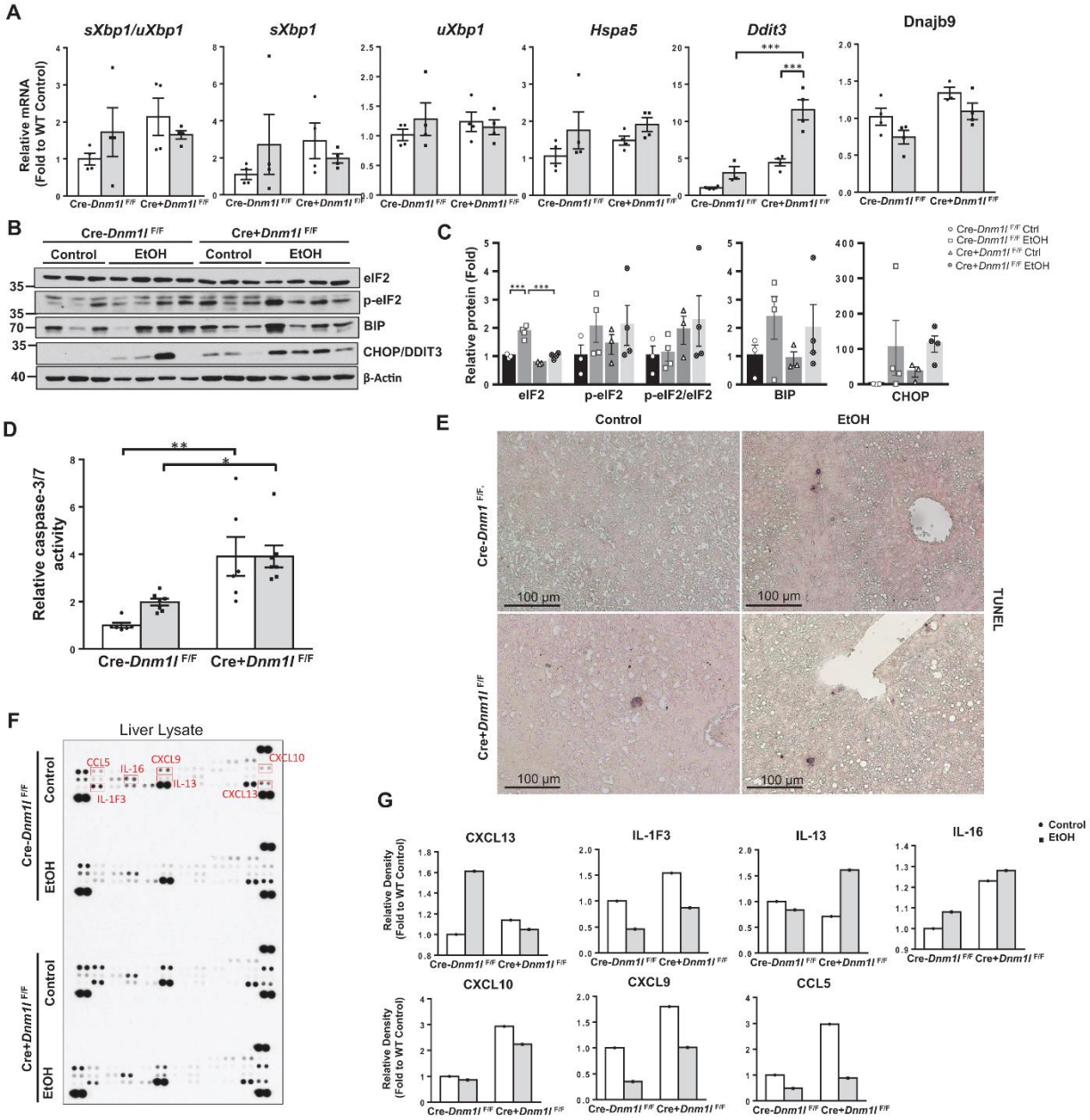

Figure S15. Alcohol-fed L-DRP1 KO mice may have mild hepatic ER stress, hepatocyte apoptosis and elevation of a sub-group of cytokines/chemokines. (A) qPCR analysis of ER-stress related genes. (B) Total liver lysates were subjected to western blot analysis. (C) Density analysis of (B). (D) Caspase 3/7 activity from total liver lysate was measured using Asp-Glu-Val-Asp (DEVD) substrate. (E) Representative TUNNEL staining images. (F) Pooled mouse liver lysate were subjected to mouse cytokine antibody array kit (Cat. ARY006) for the detection of 40 different cytokines and chemokines (n=4 mice). (G) Density of selected cytokines/ chemokines.

Supplemental Figure 16

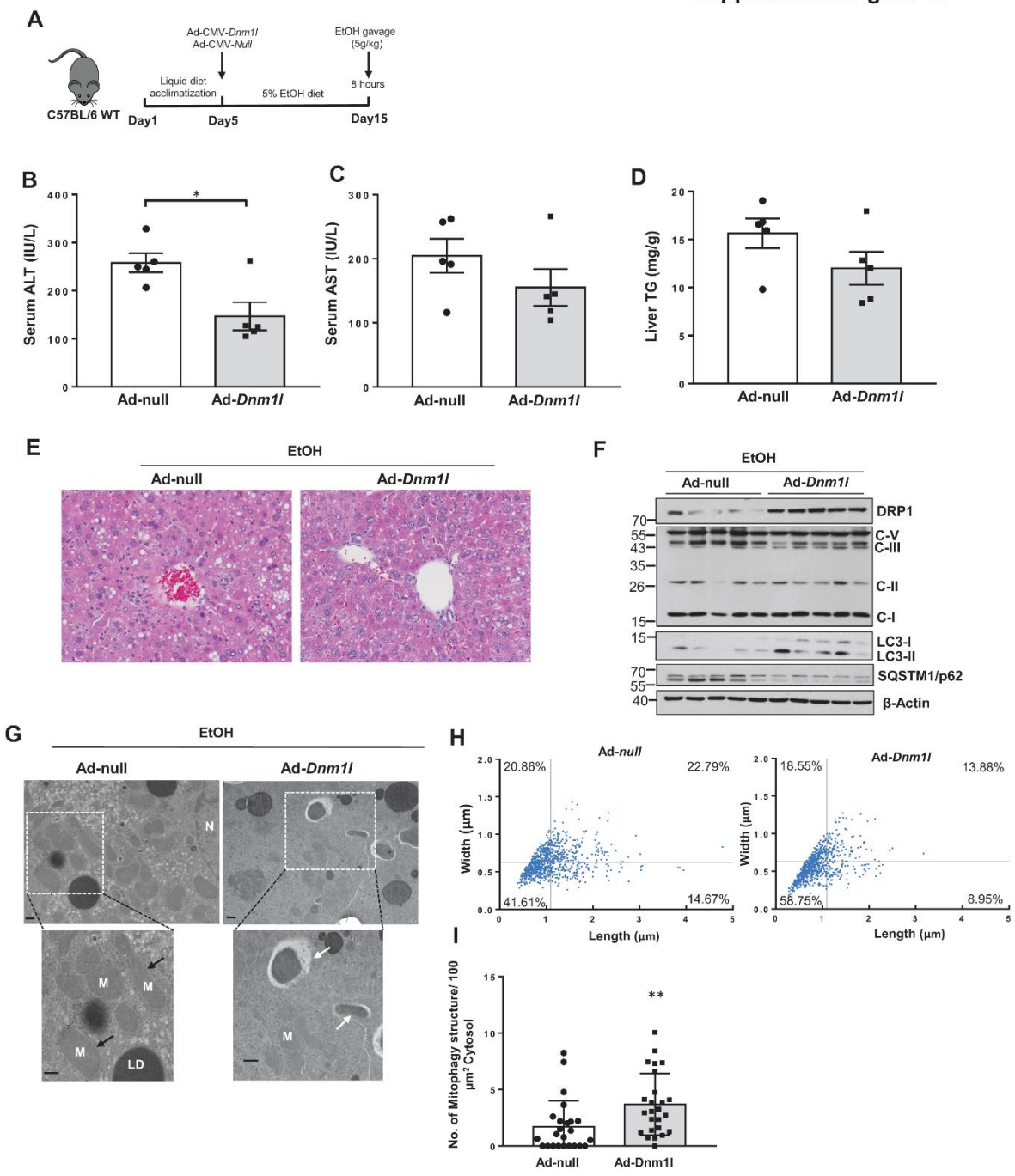

Figure S16. Restoration of *Dnm1l* attenuates Gao-binge alcohol feeding-induced liver injury by increasing mitochondria fragmentation and mitophagy. Male WT C57BL/6J mice (2-3 months old) were subjected to Gao-binge alcohol feeding. Ad-null or Ad-*Dnm1l* ($5x10^8$ PFU/mouse, i.v.) were injected on Day 5, one day before the alcohol diet. Serum ALT and AST levels are shown (A-B). (C) Liver TG levels were measured. Data are presented as means± SEM (n=5). (E) Representative liver H&E staining. (F) Total liver lysates were subjected to western blot analysis. (G) Representative mouse liver EM images. Black arrows denote

megamitochondria, white arrows denote mitophagosome. (H) Mitochondrial length and width from (G) were measured using Image-Pro Plus software. The reference lines in the graph represent the average values in the Ad-null group. At least 15 different fields' mitochondria (total number 800-1000) from 2-3 mice were quantified in each group. (I) Number of mitophagosome structure quantified from (G). Data are presented as means± SD. *$p<0.05$; **$p<0.01$; two-tailed Student's t-test.

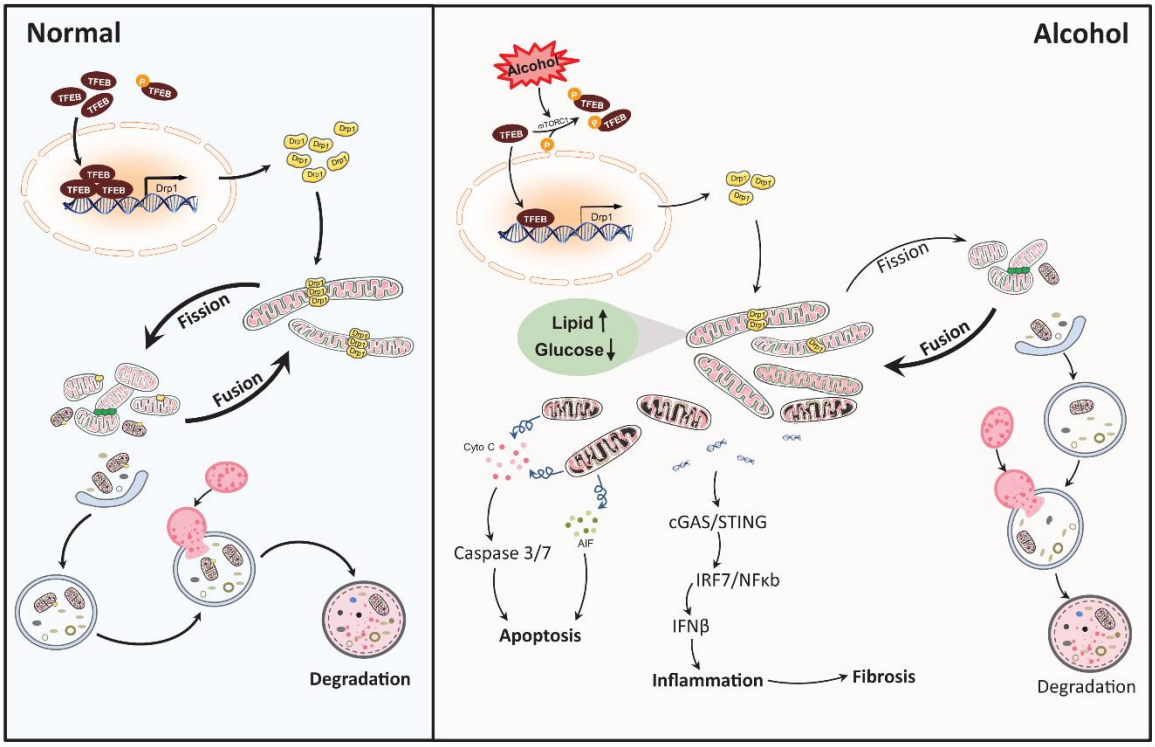

Figure S17. A proposed working model illustrating the role of mitochondrial dynamics in ALD. In normal conditions, dysfunctional mitochondria are fragmented and removed by mitophagy, a selective autophagic process that favors degrading small-sized mitochondria. Alcohol impairs TFEB function and inhibits the expression of mitochondrial fission protein DRP1, resulting in the accumulation of megamitochondria with increased mitochondria bioenergetics and shifted energy supply as an adaptive response. Chronic loss of DRP1 leads to mitochondrial maladaptive with increased release of mitochondrial apoptotic factors, mtDNA release, and cGAS-STING-IRF3/7-mediated innate immune response and aggravated liver injury.

DRP1, dynamin-related protein 1; TFEB, transcriptional factor EB; AIF, apoptosis-inducing factor; cyto C, cytochrome C; cGAS, cyclic GMP-AMP Synthase; STING, Stimulator of Interferon Genes; IRF7, Interferon Regulatory Factor 7; NF-κB, nuclear factor kappa light chain enhancer of activated B cells.

References

1. Rom O, Liu Y, Liu Z, et al. Glycine-based treatment ameliorates NAFLD by modulating fatty acid oxidation, glutathione synthesis, and the gut microbiome. Sci Transl Med 2020;12.
2. Rom O, Xu G, Guo Y, et al. Nitro-fatty acids protect against steatosis and fibrosis during development of nonalcoholic fatty liver disease in mice. EBioMedicine 2019;41:62-72.
3. Hochberg Y, Benjamini Y. More powerful procedures for multiple significance testing. Stat Med 1990;9:811-8.
4. Metsalu T, Vilo J. ClustVis: a web tool for visualizing clustering of multivariate data using Principal Component Analysis and heatmap. Nucleic Acids Res 2015;43:W566-70.
5. Mehlem A, Hagberg CE, Muhl L, et al. Imaging of neutral lipids by oil red O for analyzing the metabolic status in health and disease. Nat Protoc 2013;8:1149-54.
6. Liangpunsakul S, Haber P, McCaughan GW. Alcoholic Liver Disease in Asia, Europe, and North America. Gastroenterology 2016;150:1786-97.
7. Wang H, Ni HM, Chao X, et al. Double deletion of PINK1 and Parkin impairs hepatic mitophagy and exacerbates acetaminophen-induced liver injury in mice. Redox Biol 2019;22:101148.
8. Ni HM, Du K, You M, et al. Critical role of FoxO3a in alcohol-induced autophagy and hepatotoxicity. Am J Pathol 2013;183:1815-1825.
9. Chao X, Wang S, Zhao K, et al. Impaired TFEB-Mediated Lysosome Biogenesis and Autophagy Promote Chronic Ethanol-Induced Liver Injury and Steatosis in Mice. Gastroenterology 2018;155:865-879 e12.
10. Ni HM, McGill MR, Chao X, et al. Removal of acetaminophen protein adducts by autophagy protects against acetaminophen-induced liver injury in mice. J Hepatol 2016;65:354-62.
11. Smedsrod B, Pertoft H. Preparation of pure hepatocytes and reticuloendothelial cells in high yield from a single rat liver by means of Percoll centrifugation and selective adherence. J Leukoc Biol 1985;38:213-30.
12. West AP, Khoury-Hanold W, Staron M, et al. Mitochondrial DNA stress primes the antiviral innate immune response. Nature 2015;520:553-7.
13. Li T, Matozel M, Boehme S, et al. Overexpression of cholesterol 7alpha-hydroxylase promotes hepatic bile acid synthesis and secretion and maintains cholesterol homeostasis. Hepatology 2011;53:996-1006.